

CHEMISTRY

AN ASIAN JOURNAL

www.chemasianj.org

Accepted Article

Title: 3D Graphene-Carbon Nanotube Hybrid Supported the Coupled Co-MnO Nanoparticles as Highly Efficient Bifunctional Electrocatalyst for Rechargeable Zn-Air Battery

Authors: Chaoqi Zhang, Fantao Kong, Yu Qiao, Qingbiao Zhao, Aiguo Kong, and Yongkui Shan

This manuscript has been accepted after peer review and appears as an Accepted Article online prior to editing, proofing, and formal publication of the final Version of Record (VoR). This work is currently citable by using the Digital Object Identifier (DOI) given below. The VoR will be published online in Early View as soon as possible and may be different to this Accepted Article as a result of editing. Readers should obtain the VoR from the journal website shown below when it is published to ensure accuracy of information. The authors are responsible for the content of this Accepted Article.

To be cited as: *Chem. Asian J.* 10.1002/asia.202000913

Link to VoR: <https://doi.org/10.1002/asia.202000913>

A Journal of



A sister journal of *Angewandte Chemie*
and *Chemistry – A European Journal*

WILEY-VCH

3D Graphene-Carbon Nanotube Hybrid Supported the Coupled Co-MnO Nanoparticles as Highly Efficient Bifunctional Electrocatalyst for Rechargeable Zn-Air Battery

Chaoqi Zhang^[a], Fantao Kong^[a], Yu Qiao^[a], Qingbiao Zhao^{*[b]}, Aiguo Kong^{*[a]} and Yongkui Shan^{*[a]}

[a] C. Zhang, F. Kong, Y. Qiao, A. Kong, Y. Shan.
School of Chemistry and Molecular Engineering
East China Normal University
Shanghai 200241 (China)
E-mail: agkong@chem.ecnu.edu.cn
ykshan@chem.ecnu.edu.cn

[b] Q. Zhao.
Department of electronic Science
East China Normal University
Shanghai 200241 (China)
E-mail: qbzha@ee.ecnu.edu.cn

Supporting information for this article is given via a link at the end of the document.

Abstract: The development of high-efficiency and low-cost catalysts is one of the core and important issues to improve the efficiency of electrochemical reactions on electrodes, and it is also the goal we ultimately pursue in the commercialization of large-scale clean energy technologies, such as metal-air batteries. Herein, nitrogen-doped graphene oxide (GO)-carbon nanotubes (CNTs) hybrid network supported the coupled Co/MnO nanoparticles (Co/MnO@N-C) catalyst was prepared with a hydrothermal-pyrolysis method. The unique three-dimensional network structure of substrate allowed for the uniform dispersion of Co-MnO nanoparticles in the carbon skeleton. These characters enable the Co/MnO@N-C to possess the excellent bifunctional electrocatalysts. In alkaline electrolyte, the Co/MnO@N-C presents the outstanding oxygen evolution reaction (OER) performance comparable to the commercial RuO₂ catalyst and the exceedingly good oxygen reduction reaction (ORR) activity with positive half-wave potential of 0.90 V vs. RHE outperforming commercial Pt/C (0.84 V vs. RHE) and the recently reported analogous electrocatalysts. When it is applied to the homemade Zn-air battery, such a non-noble metal electrocatalyst can deliver the better power density, specific capacity and cycling stability than mixed Pt/C and RuO₂ catalyst, and exhibits a wide application prospect and great practical value.

Introduction

Development and research of non-precious metal electrocatalyst with the high performance and cost-effectiveness for oxygen or hydrogen transformation hold great promise for the commercialization of the renewable energy techniques and responding to the energy and environment crisis.^[1] Related research efforts have become extensive and a good deal of the non-precious metal electrocatalysts with high efficiency has been prepared by a variety of the synthesis techniques using a great diversity of precursors.^[2] Among the reported non-precious metal electrocatalysts, the transition metal-based electrocatalysts show the remarkable catalytic performance for oxygen reduction reaction, oxygen evolution reaction (OER), hydrogen evolution reaction (HER) and all water splitting reaction.^[3] Particularly, the cobalt-based electrocatalysts have

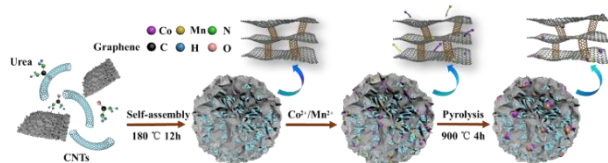
attracted a lot of interest and become one of the most hopeful candidates to substitute Pt-based catalysts.

The fruitful researches have been carried out to demonstrate the high activities of the Co-based catalyst for catalyzing ORR and OER. Generally, these reported Co-based catalysts could be roughly divided into the following categories: metal cobalt nanoparticles (NPs) supported on carbon substrate,^[4] Co-N co-doped materials,^[5] cobalt compounds (Co₃O₄, Co₉S₈, Co_xP),^[6] Co-based non-noble metal alloy (FeCo, CoMn...)^[7] and the single atom cobalt.^[8] Almost of these catalysts exhibit the favorable electrocatalytic performances for ORR. The half-wave potential ($E_{1/2}$) of cobalt-based catalyst Fe_{0.3}Co_{0.7}/NC with the highest activity is 880 mV vs RHE and 20 mV higher than that of commercial Pt/C catalyst ($E_{1/2}$ = 860 mV vs RHE), which indicate that Co-based catalyst is a kind of good electrode material with great potentialities of development. However, durability and activity of the cobalt-based electrocatalysts were well below the required levels for the large-scale production and commercial operation of the renewable energy techniques.

The carbon-based materials such as graphene and carbon nanotube have great potential in the field of the electrocatalysis because of their lower prices, excellent stability and electrochemical properties.^[9] In addition, it has been reported in the literature that the three-dimensional structure formed by the hybridization of the graphene (Gph) and carbon nanotubes (CNTs) can overcome the spontaneous agglomerate of them. On this basis, the hybrid materials of Gph with CNTs are considered the superior supports for the active species in the electrocatalysts. Here, the 2D graphene oxide and 1D carbon nanotube used as the carbon sources and building-blocks, the urea as the nitrogen source, the 3D N-doped graphene oxide (GO)-carbon nanotubes (CNTs) hybrid materials (N-DG/C) with the hierarchically porous structure are synthesized and act as the supports to capture and scatter the coupled Co-MnO nanoparticles. The obtained catalysts, N-DG/C supported the coupled Co-MnO nanoparticles (Co/MnO@N-C), has an excellent catalytic performance superior to Pt/C and other similar materials in 0.1 M KOH solution and comparable to commercial Pt/C in 0.1 M H₂SO₄ solution for ORR. Moreover, the prepared catalysts also possess the higher catalytic activity for OER than

the widely-used IrO_2 catalyst. The Zn-air battery assembled with the Co/MnO@N-C showcase exceedingly good performance compared to those with the mixed Pt/C and RuO_2 catalyst and promising market perspective.^[10]

Results and Discussion



Scheme 1. Schematic representation for the synthesis of Co/MnO@N-C electrocatalysts.

Scheme 1 schematically presents the experimental process for synthesizing Co/MnO@N-C through the hydrothermal-pyrolytic method.^[2c,11] First, 3D N-doped graphene-carbon nanotube hybrid (N-DG/C) with network structure is assembled through the hydrothermal treatment using graphene oxide and carbon nanotubes as the carbon source and urea as the nitrogen source. Then $\text{CoCl}_2 \cdot 6(\text{H}_2\text{O})$ and $\text{MnCl}_2 \cdot 4(\text{H}_2\text{O})$ were supported on the prepared N-DG/C by ultrasonic dispersion, and followed by the pyrolysis at high temperature under N_2 atmosphere to obtain the N-DG/C supported the coupled Co/MnO nanoparticles (Co/MnO@N-C).

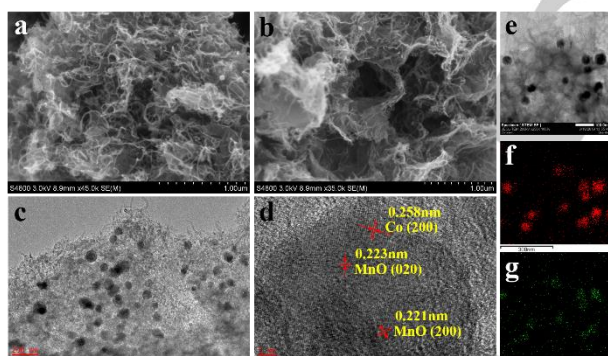


Figure 1. a), b) SEM, c) TEM, d) HR-TEM images and e)-g) the corresponding EDS mappings of Co and Mn elements of Co/MnO@N-C.

The scanning electron microscopy (SEM) and transmission electron microscopy (TEM) were used to observe the morphology and microstructure of the prepared materials. As displayed in Fig. 1a, the obtained Co/MnO@N-C possesses the loosened foam-like structures constructed by the graphene oxides and nanotubes. Abundant channels and hierarchical pore structures can be seen from Fig. 1b, which are beneficial for the dispersion of the nanoparticles and the mass transfer in electrocatalytic process. From the TEM image (Fig. 1c and Fig. s5), it shows that the Co and MnO nanoparticles disperse uniformly on the foam-like substrate and the root of individual CNT is directly connected to the graphene surface, which is consistent with the results reported previously by us.^[11] The

high-resolution TEM image (Fig. 1d) presents the apparent lattice fringes with the interplanar spacings of 0.221, 0.223 and 0.258 nm, which represent the (200) and (020) facets of MnO and the (200) facet of Co.^[2d,12] The TEM mapping (Fig. 1e-g and Fig. S4) showing the elemental distribution of Co, C, N, O and Mn illustrates that Co and Mn are located in the same nanoparticle and the distribution of C, N, O elements is uniform. These phenomena clearly certify the formation of the coupled Co-MnO nanoparticles, which provide the material basis of the high-efficient catalytic activity coming from the synergistic effect of Co and MnO nanoparticles.

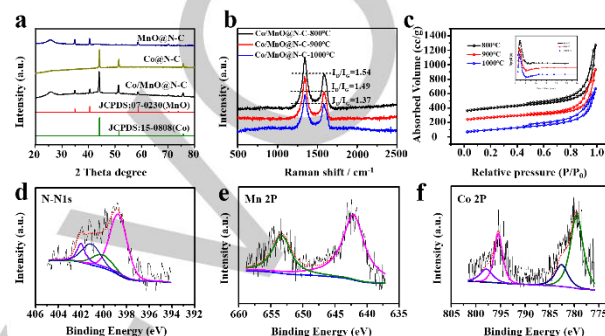


Figure 2. a) The XRD patterns of MnO@N-C, Co@N-C and Co/MnO@N-C; b) Raman spectra of Co/MnO@N-C-X (X=800, 900, 1000); c) N_2 adsorption and desorption isotherms of Co/MnO@N-C-X; The corresponding pore size distribution curves of Co/MnO@N-C (inset); d) N_{1s} e) Mn_{2p} f) Co_{2p} XPS spectra of the Co/MnO@N-C-900.

X-ray powder diffraction (XRD) pattern was utilized to investigate the crystal structure of the prepared materials Co@N-C, MnO@N-C and Co/MnO@N-C. As shown in Fig. 2a, the characteristic peaks of Co@N-C and MnO@N-C indicate the existence of the cubic phase of metal Co (JCPDS card no.15-0808) and MnO (JCPDS card no.07-0230). In the characteristic patterns of Co/MnO@N-C, three diffraction peaks located at 44.2° , 51.4° and 75.7° correspond to the (111), (200) and (220) lattice planes of the cubic Co and centered at 34.8° , 40.5° , 58.6° , 70.2° and 73.8° correspond to the (111), (200), (220), (311) and (222) planes of the cubic MnO. The results testify that Co^{2+} transforms into Co metal and MnCl_2 transform into MnO in the pyrolysis process. Raman scattering technique was used to investigate the degree of graphitization of the prepared materials. Raman spectra of Co/MnO@N-C-X (X=800, 900, 1000) obtained by pyrolysis at 800, 900 and 1000°C show two strong characteristic peaks of D and G bands at 1350cm^{-1} and 1590cm^{-1} , respectively (Fig. 2b)^[13] Theoretically, the G band is attributed to the stretching mode of the C-C bond (sp^2 carbon atom) in the graphite structure (such as carbon nanotube, graphene and graphite nanosheets). The D band is related to the vibrational mode of sp^3 carbon atom from the disordered structure in the carbon materials.^[13,14] The peak intensity ratio between D and G bands (I_D/I_G) is used to estimate the content of defect or the degree of graphitization of carbon materials.^[15] The I_D/I_G values of Co/MnO@N-C-800, -900 and -1000 are 1.54, 1.49 and 1.37, respectively (Fig. 2b), which indicated that the degree of graphitization goes up and the content of defects (or disorder) in the graphene and carbon tube go down in the prepared materials with the pyrolytic temperature.

The N_2 adsorption-desorption isotherms of the Co/MnO@N-C-X (X=800, 900, 1000 °C) shown type-IV curve with well-defined H₃-type hysteresis loops at the relative pressure (P/P_0) range of 0.45 to 1.0, which illustrates the existence of mesoporous (Fig. 2c). The pore size distribution located at 2.25 nm was calculated from the adsorption branch based on the Barrett-Joyner-Halenda (BJH) models (inset in Fig. 2c). Co/MnO@N-C-900 presented the higher specific surface area (443 m² g⁻¹) and pore volume (1.54 cm³ g⁻¹) than that of Co/MnO@N-C-800 (432 m² g⁻¹, 1.27 cm³ g⁻¹), Co/MnO@N-C-1000 (358 m² g⁻¹, 0.364 cm³ g⁻¹) (Table S1) and other similar materials.^[16] When the pyrolysis temperature increased to 1000°C, many stacked holes collapsed and thus resulted into the decreasing of the surface area. The larger specific area and appropriate pore structure would be advantageous to improve the electrocatalytic performance of the catalysts.

The elemental compositions and bonding character of component elements in the surface of the prepared materials are explored by XPS spectrum. Survey XPS spectrum in Fig. S1 show that the Co/MnO@N-C-900 is composed the Co (1.34%), Mn (2.41%), N (1.49%), O (4.25%) and C (90.51%). The high-resolution of N 1s spectrum (Fig. 2d) could be split into four peaks corresponding to pyridinic N (398.4 eV), pyrrolic N (400.4 eV), graphitic N (401.1 eV) and oxidized N (402.3 eV).^[17] These data prove that nitrogen can be doped into carbon skeleton during the hydrothermal procedure. The Mn 2p XPS spectrum (Fig. 2e) displays two obvious peaks at binding energies of 641.2 eV and 653.1 eV, corresponding to Mn²⁺ 2p_{3/2} and Mn²⁺ 2p_{1/2}, which confirm the formation of MnO.^[18] The Co 2p spectrum (Fig. 2f) of Co/MnO@N-C-900 reveals that the binding energy of Co 2p_{1/2} (795.4 eV) and Co 2p_{3/2} (779.5 eV) fall in the metal Co 2p energy region, indicating existence of the elemental Co in the catalysts. The peaks at 797.7 eV and 782.6 eV in Fig. 2f suggest the presence of a very small amount of Co²⁺ in the Co/MnO@N-C-900.^[19]

Tafel slope curves of OER on Co@N-C, MnO@N-C and Co/MnO@N-C-X samples; i) LSV polarization curves of OER on Co/MnO@N-C-900 samples before and after 2000 CV cycles. 0.1 M KOH is used as the electrolyte during all the measurement.

To assess the electrocatalytic performance of the prepared materials for oxygen reduction reaction (ORR), the cyclic voltammetry (CV) curves of the Co/MnO@N-C-900 as the electrode catalysts was shown in Fig. 3a and present an obvious peak at 890 mV vs. RHE in O₂-saturated 0.1 M KOH solution, but not in N₂-saturated solution, which indicated the efficient ORR activity of the Co/MnO@N-C. The measurement results of LSV in Fig. 3b show the onset potential and the half-wave potential of ORR on the Co/MnO@N-C-900 is 1020 mV and 900 mV vs. RHE and more positive than those on the Co@N-C, the MnO@N-C, the Co/MnO@N-C-800 and Co/MnO@N-C-1000. Meanwhile, more remarkable, the half-wave potential on Co/MnO@N-C-900 was 60 mV more positive than that on the commercial Pt/C catalyst ($E_{1/2} = 840$ mV vs. RHE) and higher than those on other similar materials reported in the literature recently (Table S2).^[2e,8,16a,16c,20] The corresponding Tafel slope transferred from LSV curves was shown in Fig. 3c, which reflected the behavior of ORR kinetics. The Tafel slope of ORR on Co/MnO@N-C-900 (49.2 mV dec⁻¹) was smaller than those on Pt/C (59.8 mV dec⁻¹), Co@N-C (64.8 mV dec⁻¹), MnO@N-C (80.2 mV dec⁻¹), Co/MnO@N-C-800 (64.2 mV dec⁻¹) and Co/MnO@N-C-1000 (65.9 mV dec⁻¹), indicating the faster kinetics of ORR on Co/MnO@N-C-900. The apparent number of electrons transferred in the ORR was calculated with Koutecky-Levich (K-L) equation.^[17] Fig. 4d shown the LSV curves at different rotation rate of the electrode (400 to 2500 rpm). And the inset of Fig. 3d presented the relation of linear change of j^{-1} and $\omega^{-1/2}$ in the potential range from 0.1 to 0.6V. According to the slope of the Koutecky-Levich plots at different potentials, the number of electron transferred was counted to be 3.9, illustrating that ORR occur mainly by a 4e⁻ reduction pathway from O₂ to OH⁻ on the Co/MnO@N-C electrode in the alkaline medium.

The methanol resistance properties of Co/MnO@N-C-900 and Pt/C were investigated with time-current testing technology in O₂-saturated alkaline media. As shown in Fig. 3e, after methanol was added into the electrolyte, there was no obvious decline of current density for Co/MnO@N-C-900 compared with Pt/C. This result reflected the outstanding methanol resistance performance of Co/MnO@N-C electrode. The stability of the catalyst was assessed by repeatedly CV scanning for 5000 cycles. As shown in Fig. 3f, the initial CV curve on Co/MnO@N-C-900 could coincide exactly with the final one after 5000 cycles, indicating the good stability of the Co/MnO@N-C in 0.1 M KOH solution and which was apparently higher than that of Pt/C (Fig. S2).

Furthermore, the electrocatalytic performance of Co/MnO@N-C for ORR in acidic medium also was investigated by the same techniques as those used in the alkaline media mentioned above. The experimental results demonstrate that the Co/MnO@N-C-900 possess the obvious ORR activity (Fig. S3a and 3b), the favorable stability (Fig. S3e) and the excellent methanol resistance (Fig. S3f) and can efficiently catalyze the ORR with a fast-kinetic rate (Fig. S3c) by the 4e⁻ reduction pathway from O₂ to H₂O (Fig. S3d, inset) in 0.5 M H₂SO₄ solution. The onset potential (E_{onset}) and the half-wave potential ($E_{1/2}$) of ORR on the Co/MnO@N-C-900 are 880 mV and 780

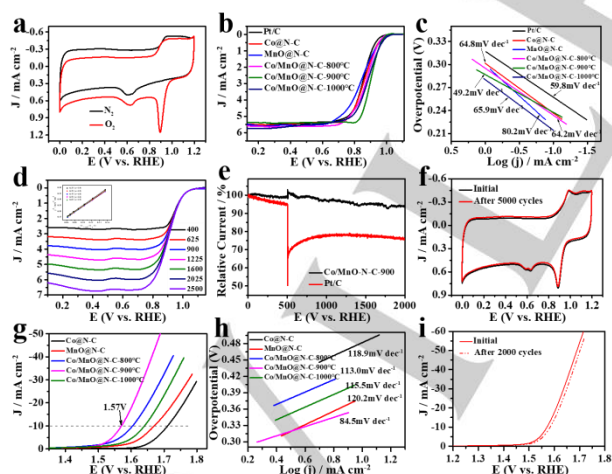


Figure 3. a) CV curves of Co/MnO@N-C in O₂ and N₂ saturated electrolyte; b) LSV polarization curves of ORR on Pt/C, Co@N-C, MnO@N-C and Co/MnO@N-C-X samples at 1600 rpm; c) Tafel slope curves of ORR on Pt/C, Co@N-C, MnO@N-C and Co/MnO@N-C-X samples; d) LSV curves at different rotation rates with the scan rate of 5 mV s⁻¹; K-L plot and the corresponding electron transfer numbers (inset) (n) at various potentials for Co/MnO@N-C; e) Current-time (i-t) chronoamperometric response of Co/MnO@N-C-900 and Pt/C with the addition of methanol (3 wt %); f) The stability test results for Co/MnO@N-C-900 by CV curves; g) LSV polarization curves of OER on Co@N-C, MnO@N-C and Co/MnO@N-C-X samples; h)

mV vs. RHE in 0.5 M H₂SO₄ and was only 40 mV and 30 mV lower than those on commercial Pt/C ($E_{\text{onset}} = 920$ mV; $E_{1/2} = 810$ mV vs. RHE) (Fig. S3b). These results indicate that the Co/MnO@N-C-900 present the ideal catalytic performance for ORR and excellent stability in acidic condition.

The research results for the OER performances of the Co@N-C, MnO@N-C and Co/MnO@N-C prepared by pyrolyzed at different temperatures were manifested in Fig. 3g-i. From the LSV curves in Fig. 3g, it was seen that the Co/MnO@N-C-900 possessed an ideal OER activity with the overpotential ($E_{j=10}$) of 1.57 V at the current density of 10 mA cm⁻², which was lower than the Co@N-C (1.71 V), MnO@N-C (1.67 V), Co/MnO@N-C-800 (1.64 V) and Co/MnO@N-C-1000 (1.61 V) catalysts and only 0.02 V higher than RuO₂ catalyst ($E_{j=10} = 1.55$ V). Moreover, OER activity of the Co/MnO@N-C-900 outperforms the most cobalt and manganese composite materials reported in the literature^[21]. The Tafel slope of OER on Co/MnO@N-C-900 is 84.5 mV dec⁻¹ and lower than those on Co@N-C (118.9 mV dec⁻¹), MnO@N-C (120.3 mV dec⁻¹), Co/MnO@N-C-800 (113.0 mV dec⁻¹) and Co/MnO@N-C-1000 (115.5 mV dec⁻¹) (Fig. 3h), showing an excellent kinetic capability of OER on the Co/MnO@N-C-900 catalyst. After 2000 CV cycles, the polarization curve of the Co/MnO@N-C-900 shows a slightly degradation compared with the initial curve, as shown in Fig. 3i, illustrating the outstanding stability of the Co/MnO@N-C-900 for OER in the alkaline solutions, and which was higher than those of many noble metal-based catalysts^[10,22] as well as the reported Co-based catalysts.^[2a,21a,23]

Co/MnO@N-C-800, and Co/MnO@N-C-1000 ($R_{\text{ct}} = 29 \Omega$), N-DG/C ($R_{\text{ct}} = 41 \Omega$) and Pt/C ($R_{\text{ct}} = 57 \Omega$), illustrating the low charge-transfer resistance and the fast charge transfer rate on the Co/MnO@N-C-900 catalyst^[24]. The electrochemical active areas (ECSA) for Co@N-C, MnO@N-C, Co/MnO@N-C were calculated by Parsons-Zobel plot method.^[25] Within the range of the potential where no electrochemical reaction occurs, the limiting current density (j) is measured at different scanning rate (v) and the results (CV curves) were shown in Fig. 4b-d present the CV curves at different scanning rates, displaying that the limiting current density increases with the rising of the scanning rate. According to the CV curves, the linear relation between j and v can be written as:

$$j = vC_d$$

And the slopes (C_d) of the linear equation were represented in Fig. 4e-g. ECSA was further given through the following equation:

$$\text{ECSA} = \frac{C_d}{A \times C_s}$$

where A is the amount of the material coating on the surface of electrode (mg·cm⁻²), C_s is an empirical constant representing the capacitance per unit area (40mF·cm⁻²)^[17]. The corresponding values are summarized in Table S3. ECSA of the Co/MnO@N-C-900 is 1470.88 cm²·mg⁻¹ and larger than those of Co@N-C (1376.01 cm²·mg⁻¹) and MnO@N-C (1183.80 cm²·mg⁻¹). From this, it could be found that the combination of Co and MnO in the Co/MnO@N-C not only change the chemical component of the catalyst, but also increase its ECSA.

Moreover, the electrochemical reaction current density (J_k) on the catalysts was calculated with equation below.^[26]

$$J_k = \frac{J_D \times J}{J_D - J}$$

where J_D is the limiting current density and J is the measured current density. The calculated results were shown in Fig. 4h. The electrochemical reaction current density on the Co/MnO@N-C-900 at 0.85 V is 21.3 mA cm⁻², the higher than those on other prepared catalysts and 3.2 times that on Pt/C (6.58 mA cm⁻²). This phenomenon implies that the Co/MnO@N-C-900 maybe possesses the active site with very higher activity and the higher density of the active sites.

The Tafel curves for ORR on different catalysts (Fig. 4i) show the same curve shape between Co@N-C and Co/MnO@N-C-900, indicating the same kinetic processes of electrochemical reaction on them. This fact demonstrates that the cobalt was acted as the major catalytic center and the manganese oxide was used as cocatalyst. On the other hand, some studies have proved that MnO can efficiently promote adsorption of the oxygen species on the surface of the catalysts for oxygen transformation reaction.^[23,27] For this reason, we reckon that the MnO can facilitate the enrichment of oxygen and transferring oxygen species into Co active center and Co catalyze oxygen transformation reaction on the surface of the Co/MnO@N-C-900.

Such synergistic effect between Co and MnO dramatically enhances the performance of catalysts for the oxygen transformation reactions. From what we have mentioned above, it can be clearly seen that the excellent catalytic performance of Co/MnO@N-C-900 should originate in the higher efficient active center resulting from the synergistic effect between Co and MnO, fast charge transfer rate and the higher density of the active sites on it.

To further explore the potential for practical application of the prepared catalysts, the home-made rechargeable zinc-air

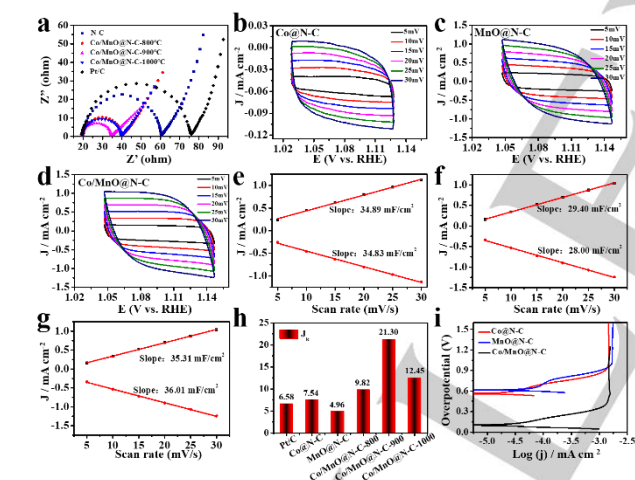


Figure 4. a) Nyquist plots of N-DG/C, Pt/C and Co/MnO@N-C-X (X=800, 900, 1000); b)-d) CV curves for Co@N-C, MnO@N-C and Co/MnO@N-C-900 in the potential range from 1.02 V to 1.16 V at scan rates of 10 mV/s, 20 mV/s, 40 mV/s, 60 mV/s, 80 mV/s and 100 mV/s; e)-g) The current densities of anode and cathode on Co@N-C, MnO@N-C and Co/MnO@N-C-900 measured at different scan rates; h) Comparison of kinetic current density at 0.85 V vs. RHE of Pt/C, Co@N-C, MnO@N-C and Co/MnO@N-C-X; i) Tafel curves for ORR on Co@N-C, MnO@N-C and Co/MnO@N-C-900. 0.1 M KOH is used as the electrolyte during all the measurement.

For further understanding the electrocatalytic behavior of the Co/MnO@N-C, the electrochemical impedance spectroscopy (EIS), Tafel curves and electrochemical active areas (ECSA) of the prepared catalysts were determined. From Nyquist plots as shown in Fig. 4a, it can be observed that the Co/MnO@N-C-900 exhibited the smaller semicircle ($R_{\text{ct}} = 14 \Omega$) than those on the

battery was assembled using carbon-fiber-cloth supported Co/MnO@N-C-900 as the air electrode. Zinc plate as the anode and 6.0 M KOH + 0.2 M Zn(CH₃COO)₂ as the electrolyte solution. As shown in Fig. 5a, the zinc-air battery impelled by Co/MnO@N-C-900 presents the open circuit potential of 1.65 V, which was higher than that by Pt/C (1.42 V). The polarization and power density curves of zinc-air battery were showed in Fig. 5b. It can be found that the battery derived from Co/MnO@N-C-900 presents a peak power density of 165 mW cm⁻², outperforming that from the Pt/C catalyst (100 mW cm⁻²). The calculated specific capacity of the zinc-air battery driven by Co/MnO@N-C based on the consumed zinc was 821 mAh g_{Zn}⁻¹, which was corresponded to an energy density of 1012 Wh kg_{Zn}⁻¹, exceeding those of Pt/C (757 mAh g_{Zn}⁻¹, 849 Wh kg_{Zn}⁻¹) (Fig. 5c). The experimental results obtained by the galvanostatic recurrent pulse technology at the constant current density of 10 mA cm⁻² in Fig. 5d demonstrate that the Co/MnO@N-C-900 based battery possesses a superior stability after continuously circulating for 45 h, whereas the Pt/C-based battery suffered an obvious decline in the discharge voltage after 30 h. Moreover, the Co/MnO@N-C-900 based battery exhibits the excellent initial round-trip efficiency of 50.4% (discharge end potential divided by charge end potential) with a voltage gap of only 1.12 V, and the energy efficiency decreases to 45.6% after circulating for 30 h. By contrast, the mixed Pt/C and RuO₂ catalyst-based battery shows an initial energy efficiency of 41.6% with a voltage gap of 1.46 V, and such efficiency decreased to 27.6% after circulating for 23 h, reflecting the superior energy efficiency and stability of the Co/MnO@N-C-900 based battery (Fig. 6e). A light-emitting diode (LED) could be powered by two serial zinc-air batteries (Fig. 5e), indicating its feasibility of practical application in the field of the clean energy techniques.

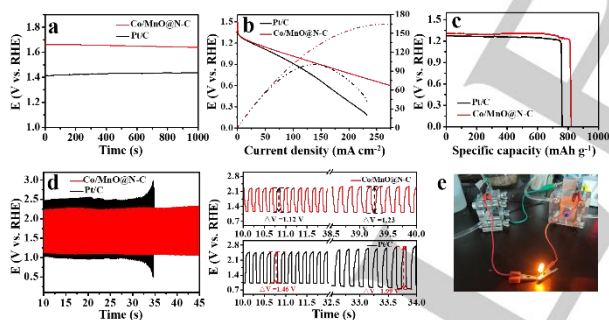


Figure 5. The Co/MnO@N-C-900- and Pt/C-based zinc-air batteries. a) Open circuit plots; b) The polarization and power density curves; c) Discharging curves at 10 mA cm⁻²; d) Galvanostatic discharge-charge cycling curve at 10 mA cm⁻² with Co/MnO@N-C-900 and Pt/C as air cathodes, respectively; (F) Photograph of the LED powered by two serial zinc-air batteries with the Co/MnO@N-C-900 as the cathode. Zincate (Zn(OH)₄²⁻) solution is used as the electrolyte

Conclusion

A facile method was proposed for synthesizing the novel carbon-based non-precious metal catalyst. The obtained catalyst Co/MnO@N-C is composed of the support with loosened foam-like structures constructed by the GO and CNTs and the coupled Co-MnO nanoparticles dispersed uniformly on the foam-like support. The synergistic effect of cobalt and manganese oxide,

the fast charge transfer rate, the larger specific area and abundant channels and hierarchical pore structures in the support endows the prepared catalyst with the excellent ORR performance in basic (half-wave potential of 900 mV vs. RHE) and acidic electrolyte (half-wave potential of 740 mV vs. RHE) and the higher OER activity (the overpotential of 1.57 V at the current density of 10 mA cm⁻²), which are superior to the commercial Pt/C and outperform the most Co based catalysts reported in the literatures. The uniformly dispersion of coupled Co-MnO nanoparticles within the porous carbon skeleton distinctly enhance the durability of the catalysts. Moreover, the Zn-air battery using Co/MnO@N-C as the cathode exhibited the excellent peak power density, specific capacity and stability, comparing with the benchmark mixed Pt/C and RuO₂ catalyst. This work provides an advanced strategy to prepare cheap and highly efficient bifunctional electrocatalyst for ORR and OER and illustrates that the prepared catalysts possess broad prospects for application in energy storage and conversion technologies.

Experimental Section

Materials

All reagents are obtained from Sinopharm Chemical Reagent Co. Ltd and used without further purification. The commercially Pt/C catalyst was used. The percentage of carbon in Pt/C is 80 wt.%.

Synthesis of graphene oxides (GO)

GO was synthesized by the modified Hummers method.^[28] Firstly, 5 g graphite were added into a three-necked flask which contained 100 mL H₂SO₄ (98%), 2.5 g P₂O₅ and 2.5 g K₂S₂O₈ and the obtained mixture was stirred at 80 °C for 6 h to finish the pre-oxidation of graphite. Then, the pre-oxidation graphite (5 g) was mixed with 98% H₂SO₄ (115 mL) in the ice bath and 15 g KMnO₄ was added into the reactor slowly with the rapid stirring to make sure that the reaction temperature was below 10 °C. After continuing to stir for 2 h at the room temperature, the graphite was oxidized completely. Next, 200 mL deionized (DI) water was added into the product of the precious step, stirring continuously until the system cooled down to the room temperature. Then 700 mL DI water and 12.5 mL H₂O₂ (30%) were poured into the mixture to wash away the residual metal oxides and their salts. The obtained product was washed with dilute hydrochloric acid solution (3%) for three times and dialysis (dialysis membrane retained molecular weight: 8000-14000 Da) for one week to get the final product.

Synthesis of nitrogen-doped graphene/carbon nanotube hybrid

The commercially multi-walled carbon nanotubes (MWCNTs) were used to synthesize nitrogen-doped graphene/carbon nanotube hybrid, whose specification is 10-30 nm in diameter, 5-15 μm in length, purity 95 wt.%. Firstly, 40 mL MWCNT suspension (1 mg/mL), 25mL GO solution (2 mg/mL) and 24 g urea were mixed and sonicated uniformly. Then the mixture was transferred to the poly(tetrafluoroethylene)(Teflon)-lined autoclave and heated at 180 °C for 12 h. The product was filtered and washed with the DI water until the filtrate was neutral. The black powder was freeze-dried in lyophilizer overnight to obtain the N-doped graphene-carbon nanotube hybrid (N-DG/C).

Synthesis of N-DG/C supported Co/MnO coupled nanoparticles (Co/MnO@N-C)

50 mg CoCl₂·6(H₂O) (2×10⁻⁴ mol) and 40 mg MnCl₂·4(H₂O) (2×10⁻⁴ mol) were mixed with the N-DG/C materials and dispersed into 20 mL ethanol

by ultrasound. The mixture was stirred at room temperature until the solvent volatilized completely. The residual solid was ground and transferred into the silica tube to be pyrolyzed at 900 °C for 4 h with a heating rate of 2 °C min⁻¹ in high-purity N₂ atmosphere, and then cooled down to ambient temperature to obtain the final product and named N-doped graphene/carbon nanotubes hybrid supported Co/MnO coupled nanoparticles (Co/MnO@N-C-900). As a contrast, N-doped graphene carbon nanotubes hybrid supported Co nanoparticles (Co@N-C), MnO nanoparticles (MnO@N-C) and coupled Co/MnO nanoparticles obtained by pyrolysis at 800 °C (Co/MnO@N-C-800) and 1000 °C (Co/MnO@N-C-1000) were synthesized with the similar method.

Electrode preparation and electrochemical measurement

Cyclic voltammetry (CV) and rotating disk electrode (RDE) techniques were conducted in a standard three-electrode system. A Pt wire served as a counter electrode, an Ag/AgCl electrode (KCl, 3.5 M) as the reference electrode and a catalyst-modified glassy carbon electrode (5.6 mm in diameter, Pine) as working electrodes. The ORR experiments were carried out in O₂-saturated 0.1 M KOH solution and 0.5 M H₂SO₄ solution at a scan rate of 5 mV s⁻¹ at the ambient temperature. The ORR current is obtained by deducting the current measured in N₂-saturated electrolyte from the current measured in the O₂-saturated electrolyte. The catalyst inks were prepared by dispersing 10 mg of catalysts in 1.28 mL alcohol solution containing 30 μL Nafion solution (5 wt %) by sonication to form a homogeneous suspension. The obtained suspension was pipetted onto a polished glassy carbon electrode surface and dried at room temperature. The mass loading on the working electrode is 0.6 mg cm⁻² in 0.1 M KOH and 0.80 mg cm⁻² in 0.5 M H₂SO₄ solutions. The commercially available Pt/C catalyst (Johnson Matthey, 20 wt % Pt) with the general loading of 20 μg Pt cm⁻² was used for comparison. The potential at which the ORR current density reached to 3 μA cm⁻² in RDE polarization curves is taken to be the ORR onset potential. The OER property was investigated in an O₂-saturated 1.0 M KOH solution at room temperature. The general loading of catalysts in the OER on the working electrode was 0.6 mg cm⁻². The benchmark IrO₂ catalyst electrodes with the same mass loading as Co/MnO@N-C working electrode was utilized for investigation and comparison. Linear Sweep Voltammetry (LSV) curves were recorded at a scan rate of 5 mV s⁻¹. All the potentials were calibrated with a reversible hydrogen electrode (RHE). The electron-transfer number (n) involved in a typical ORR process was estimated by using the Koutecky-Levich (K-L) equation.

$$\frac{1}{j} = \frac{1}{j_k} + \frac{1}{j_L} = \frac{1}{j_k} + \frac{1}{B\omega^{1/2}}$$

where j , j_k , and j_L are the measured current density, the kinetic current density, and the diffusion-limited current density, respectively, ω is the angular velocity (rad s⁻¹), and B is the Levich constant, which is determined from the slope of Koutecky-Levich plots based on Levich equation as followed:

$$B = 0.62nFC_0D_0^{2/3}v^{1/6}$$

where n is the overall number of electrons transferred in the ORR process, F is the Faraday constant, C_0 is the concentration of O₂, D_0 is the diffusion coefficient of O₂ in the electrolytes, and v is the kinetic viscosity of the electrolyte. The constant 0.2 is adopted when the rotating speed is in revolutions per minute (rpm). For ORR and OER, the Tafel slope (b) was obtained by fitting the linear part of the Tafel plots according to the Tafel equation to evaluate the kinetic performance of as-prepared catalysts for ORR and OER. Electrochemical impedance spectroscopy (EIS) was measured in the O₂-saturated 0.1 M KOH solution in the frequency range of 1000 kHz to 0.01 Hz with an amplitude of 10 mV.

Zinc-air batteries test

The Zn-air battery was prepared according to the following process.^[11a] The cathode was composed of carbon cloth supported catalyst with a loading of 5 mg cm⁻¹ and the zinc plate was used as the anode. The electrolyte was prepared by mixing 6 M KOH and 0.2 M Zn(AC)₂ to form zincate (Zn(OH)₄²⁻) solution. The power density diagram and discharge polarization curve were recorded by the Galvano-dynamic method. Galvanostatic discharge-charge cycling test were conducted at ambient temperature, and a whole cycle was consisted of a discharge and a charge procedure at a constant current (10 mA cm⁻²) and the same duration (45 h with a 10 min cycling).

Supporting information

Supporting information is available from the Wiley Online Library or from the author.

Acknowledgements

This work was financially supported by the China National Natural Science Foundation (No. 21303058), Shanghai Municipal Natural Science Foundation (No. 13ZR1412400), and the key project of Shanghai Science and Technology Committee (No. 14231200300).

Conflict of interest

The authors declare no conflict of interest.

Keywords: Co/MnO coupling NPs • 3D carbon material • bifunctional electrocatalyst • metal-air battery

- [1] a) Z. Chen, D. Higgins, A. Yu, L. Zhang, J. Zhang, *Energy Environ. Sci.* **2011**, *4*, 3167-3192; b) P. Liu, D. Gao, W. Xiao, L. Ma, K. Sun, P. Xi, D. Xue, J. Wang, *Adv. Funct. Mater.* **2018**, *28*, 1706928; c) P. Liu, J. Ran, B. Xia, S. Xi, D. Gao, J. Wang, *Nano-Micro Lett.* **2020**, *1*, 68.
- [2] a) S. Jiang, C. Zhu, S. Dong, *J. Mater. Chem. A* **2013**, *1*, 3593; b) Y. Fu, H. Yu, C. Jiang, T. Zhang, R. Zhan, X. Li, J. Li, J. Tian, R. Yang, *Adv. Funct. Mater.* **2017**, *28*, 1705094; c) X. Liu, M. Park, M.G. Kim, S. Gupta, G. Wu, J. Cho, *Angew. Chem. Int. Ed.* **2015**, *54*, 9654-9658; d) C. Kuo, I. M. Mosa, S. Thanneeru, V. Sharma, L. Zhang, S. Biswas, M. Aindow, S. P. Alpay, J. F. Rusling, S. L. Suib, J. He, *Chem. Commun.* **2015**, *51*, 5951-5954; e) G. Fu, X. Yan, Y. Chen, L. Xu, D. Sun, J. Lee, Y. Tang, *Adv. Mater.* **2018**, *30*, 1704609; f) S. Guo, Y. Yang, N. Liu, S. Qiao, H. Huang, Y. Liu, Z. Kang, *Sci. Bull.* **2016**, *61*, 68-77; g) B. Guan, Y. Lu, Y. Wang, M. Wu, X. Lou, *Adv. Funct. Mater.* **2018**, *28*, 1706738.
- [3] a) T. Meng, Y. Hao, L. Zheng, M. Cao, *Nanoscale* **2018**, *10*, 101039; b) J. Yan, L. Chen, X. Liang, *Sci. Bull.* **2019**, *64*, 20-27.
- [4] S. Dou, X. Li, L. Tao, J. Huo, S. Wang, *Chem. Commun.* **2016**, *52*, 9727-9730.
- [5] a) C. Tang, B. Wang, H. Wang, Q. Zhang, *Adv. Mater.* **2017**, *29*, 1703185; b) Y. Chen, Y. Guo, H. Cui, Z. Xie, X. Zhang, J. Wei, Z. Zhou, *J. Mater. Chem. A* **2018**, *6*, 9716-9722; c) D. Lyu, Y. Du, S. Huang, B. Y. Mollamahale, X. Zhang, S. W. Hasan, F. Yu, S. Wang, Z. Tian, P. K. Shen, *ACS Appl. Mater. Interfaces* **2019**, *11*, 39809-39819; d) J. Qian, X. Guo, T. Wang, P. Liu, H. Zhang, D. Gao, *Appl. Catal. B Environ.* **2019**, *250*, 71-77.
- [6] X.F. Lu, Y. Chen, S. Wang, S. Gao, X. Lou, *Adv. Mater.* **2019**, *31*, 1902339.
- [7] D. Yan, Y. Li, J. Huo, R. Chen, L. Dai, S. Wang, *Adv. Mater.* **2017**, *29*, 1606459.
- [8] Q. Chen, L. Yang, L. Zhou, Z. Zou, C. Chen, Z. Hu, H. Yang, *ACS Catal.* **2017**, *7*, 6864-6871.

- [9] V. Yang, R. A. Senthil, J. Pan, T. R. Kumer, Y. Sun, X. Liu, *J. Colloid Interf. Sci.* **2020**, *579*, 347-356.
- [10] M. Roca-Ayats, E. Herreros, G. García, M.A. Peña, M.V. Martínez-Huerta, *Appl. Catal. B Environ.* **2015**, *183*, 53-60.
- [11] a) F. kong, Y. Qiao, C. Zhang, X. Fan, A. Kong, K. Shan, *Nano Res.* **2020**, *13*, 401-411; b) Z. Jiang, X. Zhao, X. Tian, L. Luo, J. Fang, H. Gao, Z. Jiang, *ACS Appl. Mater. Interfaces* **2015**, *7*, 19398-19407.
- [12] a) G. Fu, X. Yan, Y. Chen, L. Xu, D. Sun, J.M. Lee, Y. Tang, *Adv. Mater.* **2018**, *30*, 1704609; b) P. Yan, J. Zheng, J. Zheng, Z. Wang, G. Teng, S. Kuppan, J. Xiao, G. Chen, F. Pan, J.G. Zhang, *Adv. Energy Mater.* **2016**, *6*, 1502455.
- [13] K.N. Kudin, B. Ozbas, H.C. Schniepp, R.K. Prud'Homme, I.A. Aksay, R. Car, *Nano Lett.* **2008**, *8*, 36-41.
- [14] M. Pimenta, G. Dresselhaus, M. S. Dresselhaus, L. G. Cancado, A. Jorio, R. Saito, *Phys. Chem. Chem. Phys.* **2007**, *9*, 1276-1290.
- [15] J. Schwan, S. Ulrich, V. Batori, S. R. P. Silva, *J. Appl. Phys* **1993**, *80*, 440-447.
- [16] a) W. Wang, H. Wang, Z. Wu, Y. Yu, M. Asif, Z. Wang, X. Qiu, H. Liu, *Electrochim. Acta* **2018**, *218*, 486-493; b) H. Cheng, J-M. Chen, Q-J. Li, C-Y. Su, A-N. Chen, J-X. Zhang, Z-Q. Liu, Y. Tong, *Chem. Commun.* **2017**, *53*, 11596-11599; c) J. Xu, H. Zhang, P. Xu, R. Wang, Y. Tong, Q. Lu, F. Gao, *Nanoscale* **2018**, *10*, 13702-13712.
- [17] F. Kong, X. Fan, A. Kong, Y. Shan, *Adv. Funct. Mater.* **2018**, *28*, 1803973.
- [18] K. Lei, X. Han, Y. Hu, X. Liu, L. Cong, F. Cheng, J. Chen, *Chem. Commun.* **2015**, *51*, 11599-11602.
- [19] Z. Wu, S. Yang, Y. Sun, K. Parvez, X. Feng, K. Mullen, *J. Am. Chem. Soc.* **2012**, *134*, 9082-9085.
- [20] A. Zhao, J. Masa, W. Xia, A. Maljusch, M.-G. Willinger, G. Clavel, K. Xie, R. Schlogl, W. Schuhmann, M. Muhler, *J. Am. Chem. Soc.* **2014**, *136*, 7551-7554.
- [21] a) G. Du, X. Liu, Y. Zong, T.S.A. Hor, A. Yu, Z. Liu, *Nanoscale* **2013**, *5*, 4657-4661; b) J. Xu, Z. Hao, X. Peibo, W. Ruofeng, T. Yinlin, L. Qingyi, G. Feng, *Nanoscale* **2018**, *10*, 13702-13712.
- [22] a) C.C. Hu, C.H. Lee, T.C. Wen, *J. Appl. Electrochem.* **1996**, *26*, 72-82; b) D.A. Cullen, K.L. More, L.L. Atanasoska, *J. Power Sources* **2014**, *269*, 671-681.
- [23] W. Wang, H. Wang, Y. Yu, Z. Wu, M. Asif, H. Liu, *Catal. Sci. Technol.* **2018**, *8*, 480-485.
- [24] H. Jin, J. Wang, D. Su, Z. Wei, Z. pang, Y. Wang, *J. Am. Chem. Soc.* **2015**, *137*, 2688-2694.
- [25] a) S. Trasatti, O. Petrii, *Pure Appl. Chem.* **1991**, *63*, 711-734; b) Y. Jia, L. Zhang, A. Du, G. Gao, J. Chen, X. Yan, CL. Brown and X. Yao, *Adv. Mater.* **2016**, *28*, 9532-9538; c) J. Kibsgaard, TF. Jaramillo, *Angew. Chem. Int. Ed.* **2014**, *531*, 14433-14437.
- [26] S. Wang, E. Iyyamperumal, A. Roy, Y. Xue, D. Yu, L. Dai, *Angew. Chem. Int. Ed.* **2011**, *50*, 11756-11760.
- [27] G. Fu, X. Yan, Y. Chen, D. Sun, J. Lee, Y. Tang, *Adv. Mater.* **2017**, *30*, 1704609.
- [28] W.S. Hummers Jr, RE. Offeman, *J. Am. Chem. Soc.* **1958**, *80*, 1339-1339.

Entry for the Table of Contents



Three-dimensional graphene-carbon nanotube hybrid supported the coupled Co-MnO catalysts could be figuratively described as the luxuriant tree with fruit, whose structure reveals the unique advantages for oxygen conversion reaction. The outstanding electrocatalytic performance employ the material with a wide application prospect in the sustainable energy conversion systems.